Novel Near-Field Radar Propagation Models for V2X Communication and Sensing

François De Saint Moulin, Christophe Craeye, Luc Vandendorpe, Claude Oestges*
ICTEAM, Université catholique de Louvain (UCLouvain), Louvain-la-Neuve, Belgium
*claude.oestges@uclouvain.be

***Abstract*—The increased carrier frequencies envisioned for future vehicle-to-vehicle or vehicle-to-infrastructure (commonly abbreviated as V2X) radar and communication networks call for adequate propagation models valid in near-field transmissions. In this paper, we propose a new radar propagation model, encompassing popular models from the literature, namely the radar equation and the Geometrical Optics (GO) approximation. First, the scattered electromagnetic fields and radar cross-sections are analytically computed by modeling the radar target as an arbitrary curved rectangular plate. Secondly, when particularized to a flat plate, our new model directly highlights not only the link between the radar equation and the GO approximation, but also the limitations of those models. We finally propose a new model based on our analytical derivations, which unifies both approaches.**

***Index Terms*—electromagnetism, near-field propagation, physical optics, radar, radar cross section.**

I. Introduction

A. Joint V2X Radar and Communication Systems

Radar and communication systems exploit the electromagnetic (EM) spectrum with specific objectives. On the one hand, radar systems are deployed in order to gather information about the environment by transmitting a known waveform. By receiving and processing the waveform echoes created by multiple targets, radars are able to estimate parameters such as the position, speed and direction of the targets. On the other hand, communication systems are deployed in order to transmit information in an unknown environment, which must also be estimated in order to compensate for impairments caused by multipath scattering.

Many existing vehicular radar applications use the 24-GHz band [1], while typical communication bands range from 410 MHz up to 5.9 GHz for the Long Term Evolution (LTE) standard. Recently, higher frequencies have been considered for both radar and communication functions. For example, the 76–77 and 77–81 GHz bands have become the new standard for automotive radar systems [1]. Similarly, 5G New Radio (NR) plans to cover new bands, first extending LTE up to 7.125 GHz, with further versions moving up to 24.25 GHz and 71 GHz [2]. In this context, both radar and communication systems are converging towards the same frequencies, leading to an increased interest in joint radar-communication technologies. An important consequence of the frequency increase is that the Fraunhofer distances associated to many use cases increase from meters to multiple hundred of meters, as the Fraunhofer distance is inversely proportional to the wavelength. In other words, at such wavelengths, most transmissions occur in the near-field region.

François De Saint Moulin is a Research Fellow of the Fonds de la Recherche Scientifique - FNRS.

Near-field communication and sensing raise therefore new challenges and opportunities, such as accurate channel modelling, channel estimation algorithms, beamfocusing, or enhanced positioning [3], [4]. The accuracy of channel models is naturally crucial in order to draw reliable conclusions about system performance. Yet, many assumptions can be found in the literature: in [5], the radar interference is assumed to decrease with the fourth power of the distance, while [6], which considers a vehicular network, assumes the radar targets to be characterized by a constant Radar Cross-Section (RCS). As shown in this paper, both assumptions may actually become questionable, depending on the considered scenarios.

B. Classical Radar and Communication Channel Models

For communication systems, the Friis equation describes the power P_C received from a transmit node at a distance R as [7]

$$P_\mathrm{C}(R) = P_e\, G_r\, \frac{c^2}{4\pi f_c^2}\, \beta^{-1}\, R^{-\alpha}, \tag{1}$$

where P_e denotes the transmitted Effective Isotropic Radiated Power (EIRP), G_r is the receive antenna gain, and f_c is the carrier frequency. A linear path-loss model is considered, with β the fixed intercept and α the path-loss exponent. For free-space propagation, $\beta = 4\pi$ and $\alpha = 2$.

Alternatively, for radar applications, the received power P_R is usually computed following the well-known radar equation [8]:

$$P_\mathrm{R,RE}(R) = P_e\, G_r\, \frac{c^2}{4\pi f_c^2}\, \beta^{-2}\, R^{-2\alpha}\, \sigma, \tag{2}$$

with σ the RCS of the target, usually modelled as a constant and distance-independant parameter. However, RCS modelling is difficult, and often inaccurate. Additionally, this model is only valid in the far-field, i.e. when $r >> R_\mathrm{F} = 2D^2\, f_c/c$ with R_F known as the Fraunhofer distance, and D the largest dimension of the scatterer. In many applications, e.g. automotive scenarios, this assumption is not always fulfilled. This can lead to significantly wrong conclusions about the achieved performance. Another popular model for the power received after reflection by a scatterer is based on the Geometrical

Optics (GO) approximation, which is for instance used in ray-tracing tools [9]:

$$P_{\mathrm{R,GO}}(R) = P_e\, G_r\, \frac{c^2}{4\pi f_c^2}\, \beta^{-1}\, (2R)^{-\alpha}\, |\mathcal{R}|^2, \tag{3}$$

where $\mathcal{R}$ is the Fresnel reflection coefficient of the scatterer. For a good conductor, one may assume that $|\mathcal{R}|^2 \approx 1$. The GO approximation is similar to (1), in which the receiver would be located at a distance $2R$. However, owing to the GO approximation, the dimensions and shapes of the targets are not explicitly taken into account, as the EM waves are approximated with rays.

C. Near-Field Radar Cross-Section

RCS modelling is not recent. For example, [10] already showed that the RCSs of a sphere and a square plate in the near-field region depend upon the range and orientation of the antennas, and proposed two new definitions of the near-field RCS. The monostatic or bistatic RCS was already analysed in the near-field through a Physical Optics (PO) approach in [11], with numerical examples for rectangular and circular plates. This work was extended in [12], [13], with complex targets being decomposed into small triangular elements, such that each element propagates in the far-field. Multiple papers then extended these seminal works [14]–[17]. Finally, more complex targets, such as the back of a car at 77 GHz, were evaluated in [18]. However, because of the complexity of the RCS computation, most of these works focused on numerical analysis and measurements. By contrast, [19] proposed three-dimensional computationally efficient models based on Fresnel integrals to calculate the backscattering model of a rectangular plate, with experimental validation at 28 GHz. This work was further extended in [20], which leveraged on the proposed models to evaluate the backscattered fields with multiple oriented rectangular surfaces.

D. Paper Outline

This paper, is organized as follows. Section II details how the PO theory enables to derive analytical expressions of the scattered EM fields and RCS of arbitrarily curved rectangular targets, based on our work in [21], in which further details can be found. These expressions are then particularized to a flat target. In Section III, we illustrate how the computed RCSs vary with distance and frequency and compare the exact results with an approximation. Finally, in Section IV, we propose a new physical model based on our analytical derivations, which enables to reconcile (2) and (3) described in Section I-B.

II. Reflected Fields in Free-Space

A. General Derivations for Curved Rectangular Plates

Let us consider the scenario illustrated in Fig. 1. The coordinate system is arbitrarily taken such that a linear antenna located at $(-R, 0, 0)$ is facing a curved rectangular plate $\mathcal{S}$ of

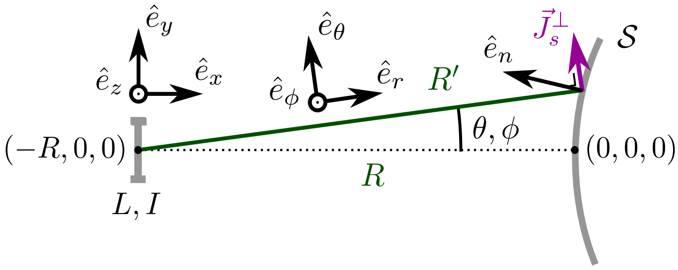

Fig. 1: Curved square plate geometry.

dimensions $D_y \times D_z$. The shape of the curved plate is modelled through a well-behaved arbitrary function $h : \mathbb{R}\times\mathbb{R}\to\mathbb{R}$ as:

$$\tilde{\mathcal{S}} \triangleq \left\{ (x,y,z)\in\mathbb{R}^3 \;\middle|\; \begin{array}{l} x = h(y,z),\ |y| \leq \dfrac{D_y}{2},\ |z| \leq \dfrac{D_z}{2} \\ h(0,0)=0, \quad \nabla h(0,0) = 0 \\ \nabla^2 h(y,z) \succeq 0,\ \dfrac{\partial^2 h}{\partial y \partial z}(0,0) = 0 \end{array} \right\}. \tag{4}$$

The third condition guarantees that the principal directions of the target are aligned with the coordinate system. In addition, the function h is taken as slowly varying w.r.t. the wavelength λ. The distance R' and the normal unit vector pointing outside the curved plate are respectively expressed as

$$R' \triangleq \sqrt{(R + h(y,z))^2 + y^2 + z^2}, \tag{5}$$

and

$$\hat{e}_n = \frac{-\hat{e}_x + \frac{\partial h}{\partial y}\,\hat{e}_y + \frac{\partial h}{\partial z}\,\hat{e}_z}{\sqrt{1 + \left(\frac{\partial h}{\partial y}\right)^2 + \left(\frac{\partial h}{\partial z}\right)^2}}. \tag{6}$$

For a transmit linear antenna of length L, the transmitted electric and magnetic fields at a distance R' of the antenna can be written as

$$\vec{E}_i = -jk\eta L I\, \frac{e^{-jkR'}}{4\pi R'}\, f(\theta)\, \hat{e}_\theta, \tag{7}$$

$$\vec{H}_i = \frac{1}{\eta}\,\hat{e}_r \times \vec{E}_i = -jkLI\, \frac{e^{-jkR'}}{4\pi R'}\, f(\theta)\, \hat{e}_\phi, \tag{8}$$

where $k = 2\pi/\lambda$ is the wave number; $\eta = 377\,\Omega$ is the free-space impedance; I is the constant current flowing through the antenna; $f(\theta)$ is the normalised antenna radiation pattern, with θ the elevation angle (equal to 0 when the direction of propagation is parallel to the antenna). The normalised antenna radiation pattern is assumed to be maximum when $\theta = \pi/2$. A polar coordinate system is associated to the antenna, with $\hat{e}_r$, $\hat{e}_\theta$, and $\hat{e}_\phi$ being respectively the radial, elevation and azimuth unit vectors.

Equations (7) and (8) are valid when $R >> 2L^2/\lambda$, which reduces to $R >> \lambda$ when L is not much larger than λ. Owing to the considered frequencies for actual radar systems (up to 81 GHz), this condition is usually fulfilled.

1) Scattered Electric Field: Following the PO approximation, the equivalent electric surface current density is expressed as

$$\vec{J}_s = 2\,\hat{e}_n \times \vec{H}_i = -2jkLI\,\frac{e^{-jkR'}}{4\pi R'}\,f(\theta)\,(\hat{e}_n \times \hat{e}_\phi), \tag{9}$$

and the backscattered electric field is computed as

$$\begin{aligned} \vec{E}_s &\approx -jk\eta \int_{\mathcal{S}} \vec{J}_s^{\perp}\,\frac{e^{-jkR'}}{4\pi R'}\,\mathrm{d}\mathcal{S} \\ &= -\frac{k^2\eta LI}{8\pi^2}\int_{\mathcal{S}} \frac{f(\theta)}{R'^2}\,e^{-j2kR'}\,\hat{e}_u\,\mathrm{d}\mathcal{S}, \end{aligned} \tag{10}$$

with $\hat{e}_u \triangleq (\hat{e}_n \times \hat{e}_\phi) - [(\hat{e}_n \times \hat{e}_\phi)\cdot\hat{e}_r]\,\hat{e}_r$. In (10), the amplitude and phase functions are defined as

$$\vec{g}(R',\theta,\phi) \triangleq \frac{f(\theta)}{R'^2}\,\hat{e}_u, \quad \psi(R') \triangleq -2kR'. \tag{11}$$

The stationary point is found by solving

$$\begin{cases} y + [R + h(y,z)]\,\dfrac{\partial h}{\partial y}(y,z) = 0 \\ z + [R + h(y,z)]\,\dfrac{\partial h}{\partial z}(y,z) = 0. \end{cases} \tag{12}$$

Solving this system of equations is not straightforward. Nevertheless, following the Fermat stationary point theorem [22], the stationary point minimises the total travelled distance and it follows geometrically that $(y_0, z_0) = (0, 0)$. This is confirmed mathematically by combining (12) with the properties (4) of h. Still relying on these properties and denoting by h_y'' and h_z'' the second derivatives of h w.r.t. y and z at the origin,

- the phase function can be approximated around the stationary point as

$$\psi(y,z) \approx -2kR - \frac{k}{R}\left[1 + Rh_y''\right]y^2 - \frac{k}{R}\left[1 + Rh_z''\right]z^2. \tag{13}$$

- the amplitude function around the stationary point is given by

$$\vec{g}(y,z) \approx \frac{1}{R^2}\,\hat{e}_y. \tag{14}$$

Consequently, defining

$$R_y \triangleq \frac{R}{1 + Rh_y''}, \quad R_z \triangleq \frac{R}{1 + Rh_z''}, \tag{15}$$

the scattered electric field (10) is approximated as

$$\begin{aligned} \vec{E}_s &\approx -\frac{k^2\eta LI}{8\pi^2}\,\frac{e^{j2kR}}{R^2}\int_{-\frac{D}{2}}^{\frac{D}{2}} e^{-j\frac{k}{R_y}y^2}\mathrm{d}y \int_{-\frac{D}{2}}^{\frac{D}{2}} e^{-j\frac{k}{R_z}z^2}\mathrm{d}z\,\hat{e}_y \\ &= -\frac{k^2\eta LI}{8\pi^2}\,\frac{e^{j2kR}}{R^2}\,\frac{2\pi}{k}\sqrt{R_yR_z} \\ &\quad \cdot F^*\left(\sqrt{\frac{2k}{\pi R_y}}\frac{D_y}{2}\right)F^*\left(\sqrt{\frac{2k}{\pi R_z}}\frac{D_z}{2}\right)\,\hat{e}_y \\ &= -k\eta LI\,\frac{\sqrt{R_yR_z}}{8\pi R^2}\,e^{j2kR}\sqrt{\Upsilon\left(\frac{R_y}{R_{\mathrm{F},y}}\right)\Upsilon\left(\frac{R_z}{R_{\mathrm{F},z}}\right)}\,\hat{e}_y, \end{aligned} \tag{16}$$

where the functions F and Υ are defined as

$$F(x) \triangleq \int_0^x e^{j\pi\frac{t^2}{2}}\,\mathrm{d}t, \quad \Upsilon(x) \triangleq 2\left(F^*\left(\sqrt{\frac{1}{2x}}\right)\right)^2, \tag{17}$$

and the Fraunhofer distances $R_{\mathrm{F},y}$ and $R_{\mathrm{F},z}$ associated to each dimension of the rectangular plate are given by

$$R_{\mathrm{F},y} \triangleq \frac{2D_y^2}{\lambda}, \quad R_{\mathrm{F},z} \triangleq \frac{2D_z^2}{\lambda}. \tag{18}$$

2) Radar Cross-Section Model: The scattered power density is computed from (16) as

$$S_s = \frac{|\vec{E}_s|^2}{2\eta} = \frac{\mathrm{EIRP}}{16\pi R^2}\,\frac{R_yR_z}{R^2}\left|\Upsilon\left(\frac{R_y}{R_{\mathrm{F},y}}\right)\Upsilon\left(\frac{R_z}{R_{\mathrm{F},z}}\right)\right|. \tag{19}$$

The RCS is then evaluated as follows:

$$\sigma \triangleq 4\pi R^2\,\frac{S_s}{S_i} = \pi R_yR_z\left|\Upsilon\left(\frac{R_y}{R_{\mathrm{F},y}}\right)\Upsilon\left(\frac{R_z}{R_{\mathrm{F},z}}\right)\right|. \tag{20}$$

Using the approximation $\Upsilon(x) \approx (x - j)/(1 + x^2)$, we obtain

$$\sigma \approx \sigma_0\,\tilde{\sigma}(R), \tag{21}$$

where $\sigma_0 \triangleq \pi R_{\mathrm{F},y}R_{\mathrm{F},z}$, and $\tilde{\sigma}$ is a distance-dependent factor,

$$\tilde{\sigma}(R) \triangleq \left[\left(1 + \left(\frac{R_{\mathrm{F},y}}{R_y}\right)^n\right)\left(1 + \left(\frac{R_{\mathrm{F},z}}{R_z}\right)^n\right)\right]^{-\frac{1}{n}}. \tag{22}$$

3) Application to Specific Shapes: Let us consider three specific shapes, namely the cylinder, the sphere, and the paraboloid.

a) Cylinder of radius ρ: For a cylinder of radius $\rho >> D_y$, curved along the z-dimension, the function h is defined as

$$h(y,z) = \rho - \sqrt{\rho^2 - z^2}. \tag{23}$$

The curvatures h_y'' and h_z'', and the distances R_y and R_z in the y- and z-axis are given by

$$h_y'' = 0 \quad \Rightarrow \quad R_y = R, \tag{24}$$

$$h_z'' = \frac{1}{\rho} \quad \Rightarrow \quad R_z = \left(\frac{1}{R} + \frac{1}{\rho}\right)^{-1}. \tag{25}$$

b) Sphere of radius ρ: For a sphere of radius $\rho >> \max(D_y, D_z)$, the function h is defined as

$$h(y,z) = \rho - \sqrt{\rho^2 - y^2 - z^2}. \tag{26}$$

The curvatures h_y'' and h_z'', and the distances R_y and R_z in the y- and z-axis become

$$h_y'' = h_z'' = \frac{1}{\rho} \quad \Rightarrow \quad R_y = R_z = \left(\frac{1}{R} + \frac{1}{\rho}\right)^{-1}. \tag{27}$$

c) Paraboloid: For a paraboloid of curvature radii $c_y >> \max(D_y, D_z)$ and $c_z >> \max(D_y, D_z)$ in the y- and z-axis, the function h is defined as

$$h(y,z) = \frac{y^2}{2c_y} + \frac{z^2}{2c_z}. \tag{28}$$

The curvatures h''_y and h''_z, and the distances R_y and R_z in the y- and z-axis are written as

$$h''_y = \frac{1}{c_y} \quad \Rightarrow \quad R_y = \left(\frac{1}{R} + \frac{1}{c_y}\right)^{-1}, \tag{29}$$

$$h''_z = \frac{1}{c_z} \quad \Rightarrow \quad R_z = \left(\frac{1}{R} + \frac{1}{c_z}\right)^{-1}. \tag{30}$$

Based on the paraboloid case, the results obtained with a cylinder of radius ρ are matched if $c_y = 0$ and $c_z = \rho$, and the results obtained with a sphere of radius ρ are matched if $c_y = c_z = \rho$. Additionally, it is equivalent to a flat plate if $c_y = c_z = \infty$.

B. Application to Flat Square Plate Targets

With a flat square plate target, the function h is defined as $h(y,z) = 0$. Thus, the curvatures are also zero, and $R_y = R_z = R$. Consequently, (16) becomes

$$\vec{E}_s \approx -\frac{k\eta LI}{8\pi R}\, e^{j2kR}\, \Upsilon\left(\frac{R}{R_{\mathrm{F}}}\right) \hat{e}_y, \tag{31}$$

and the RCS is given by

$$\sigma \triangleq 4\pi R^2 \frac{S_s}{S_i} = \pi R^2 \left|\Upsilon\left(\frac{R}{R_{\mathrm{F}}}\right)\right|^2. \tag{32}$$

From the properties of Υ described in [21], this can be asymptotically simplified, in the near- and far-field regions, as

$$\sigma \approx \begin{cases} \pi R^2 & \text{if } R << R_{\mathrm{F}}, \\ \pi R_{\mathrm{F}}^2 = 4\pi|\mathcal{S}|/\lambda^2 & \text{if } R >> R_{\mathrm{F}}, \end{cases} \tag{33}$$

where $|\mathcal{S}|$ is the surface of the plate. Hence, (33) highlights that the RCS is constant in the far-field, while it becomes a function of the distance in the near-field. Again, the RCS can be rewritten as $\sigma_0\, \tilde{\sigma}(R)$, where $\sigma_0 \triangleq \pi R_{\mathrm{F}}^2$, and

$$\tilde{\sigma}(R) \triangleq \left[1 + \left(\frac{R_{\mathrm{F}}}{R}\right)^n\right]^{-\frac{2}{n}}. \tag{34}$$

III. Numerical Analysis

Fig. 2 illustrates the evolution of the RCS with the distance for different carrier frequencies (5, 24 and 77 GHz) and different curvature radii, computed with (20) or with its approximated expression (21). The latter enables to filter out the oscillatory behaviour of the Fresnel functions, while keeping the trend of the RCS. However, at low carrier frequencies, when a constant RCS is reached, an offset is observed when using (21).

Compared to the flat target geometry ($c_y = c_z = \infty$), introducing curvatures in the y- and z-axis drastically modifies the behaviour of the RCS:

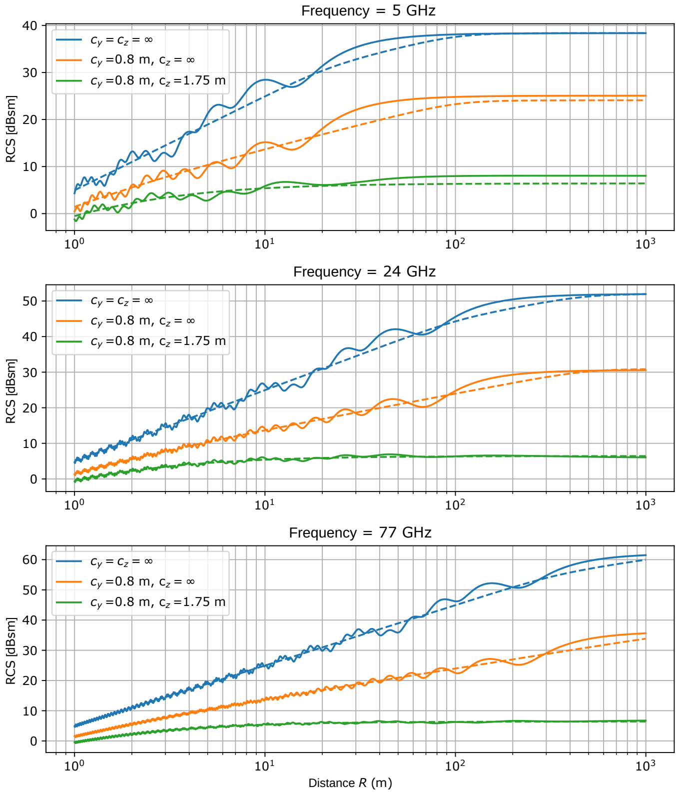

Fig. 2: RCS against distance for different carrier frequencies and different curvature radii (infinite curvature radii correspond to a flat plate; dashed lines represent (22) with $n = 4$); frequencies of 5, 24 and 77 GHz correspond to Fraunhofer distances of 33, 160, and 510 m.

- when $c_y << R_{\mathrm{F},y}$, $c_y << R$, $c_z << R_{\mathrm{F},z}$, $c_z << R$, the RCS is constant, irrespective of the Fraunhofer distance;
- when $c_y << R << c_z$ (resp. $c_z << R << c_y$), the RCS is proportional to the distance, until the Fraunhofer distance of the z-axis (resp. y-axis) is reached;
- when $R << c_y$ and $R << c_z$, the RCS is proportional to the square of the distance, until the Fraunhofer distances are reached: this is the case corresponding to the flat target.

At higher frequencies, the Fraunhofer distances are large compared to the considered distances, in both typical indoor or automotive applications. An important consequence is that the target modelling significantly impacts the radar propagation model: the RCS is either constant, proportional to the distance, or proportional to the square of the distance, depending on the considered range, frequency, and target geometry.

IV. New Propagation Model for Near-Field Radar and Communications

In Section I-B, the radar equation (2) and the GO approximation (3) have been described. If we use our novel RCS model for flat or curved geometries, in the near- and far-field regions, the equivalent propagation model reads as

$$P_{\mathrm{R}}(R) = P_e\, G_r\, \frac{c^2}{4\pi f_c^2}\, \frac{\sigma_0}{(4\pi)^2}\, \frac{\tilde{\sigma}(R)}{R^4}, \tag{35}$$

where $\sigma_0 \triangleq \pi R_{\mathrm{F},y} R_{\mathrm{F},z}$, and $\tilde{\sigma}$ is defined in (22) or (34) in the case of a square plate.

This model can also be generalised to become compatible with any path-loss model with fixed intercept β and path-loss exponent α. In that case, the definition of the RCS is adapted as

$$\sigma \triangleq \beta R^\alpha \left(\frac{S_s}{S_i}\right)^{\frac{\alpha}{2}} = \frac{\beta (R_y R_z)^{\frac{\alpha}{2}}}{2^\alpha} \left| \Upsilon\left(\frac{R_y}{R_{\mathrm{F},y}}\right) \Upsilon\left(\frac{R_z}{R_{\mathrm{F},z}}\right) \right|^{\frac{\alpha}{2}}, \tag{36}$$

with its approximated version written as

$$\begin{aligned} \sigma &\approx \frac{\beta (R_y R_z)^{\frac{\alpha}{2}}}{2^\alpha} \left[\left(1 + \left(\frac{R_y}{R_{\mathrm{F},y}}\right)^n\right) \left(1 + \left(\frac{R_{\mathrm{F},z}}{R_{\mathrm{F},z}}\right)^n\right) \right]^{-\frac{\alpha}{2n}} \\ &= \sigma_0\, \tilde{\sigma}(R), \end{aligned} \tag{37}$$

where $\sigma_0 \triangleq \beta \left(R_{\mathrm{F},y} R_{\mathrm{F},z}\right)^{\frac{\alpha}{2}} / 2^\alpha$, and the distance-dependent factor $\tilde{\sigma}$ is now defined as

$$\tilde{\sigma}(R) \triangleq \left[\left(1 + \left(\frac{R_{\mathrm{F},y}}{R_y}\right)^n\right) \left(1 + \left(\frac{R_{\mathrm{F},z}}{R_z}\right)^n\right) \right]^{-\frac{\alpha}{2n}}. \tag{38}$$

The equivalent radar propagation model is finally written as

$$P_{\mathrm{R}}(R) = P_e\, G_r\, \frac{c^2}{4\pi f_c^2}\, \frac{\sigma_0}{\beta^2}\, \frac{\tilde{\sigma}(R)}{R^{2\alpha}}. \tag{39}$$

Remarkably, our model encompasses both the radar equation model (with constant RCS) and the GO approximation-based model: it smoothly evolves from the former to the latter, both being particular cases of the combination (38)-(39).

V. Conclusion

In this paper, analytical radar propagation and RCS models are developed for curved rectangular targets, based on the PO approximation. The shape of the target can arbitrarily be defined as a continuous 3D surface. These models are valid for V2X transmissions either in the near- or far-field region. The obtained models show that the curvature of the target around the specular reflection point, i.e. the second derivatives of the shape function, defines the behaviour of the RCS with the distance and carrier frequency. When particularised to flat rectangular targets, the model unifies the radar equation and the GO approximation, showing that the former is suited for far-field applications if the RCS is assumed to be constant, whereas the latter is appropriate for near-field scenarios. In future works, RCS measurements of realistic V2X targets, e.g. the back of a real vehicle, may be carried out, to evaluate at which extent the models developed for canonical targets are actually able to predict the RCS evolution with distance and carrier frequency.

References

[1] "System reference document (SRdoc); transmission characteristics; technical characteristics for radiodetermination equipment for ground based vehicular applications within the frequency range 77 GHz to 81 GHz," *ETSI TR 103 593*, 05 2020.

[2] "5G; NR; user equipment (UE) radio transmission and reception (3GPP TS 38.101-1 version 17.5.0 release 17)," *ETSI TR 138 101-1*, 05 2020.

[3] J. An, C. Yuen, L. Dai, M. Di Renzo, M. Debbah, and L. Hanzo, "Near-field communications: Research advances, potential, and challenges," *IEEE Wireless Communications*, vol. 31, no. 3, pp. 100–107, 2024.

[4] M. Cui, Z. Wu, Y. Lu, X. Wei, and L. Dai, "Near-field MIMO communications for 6G: Fundamentals, challenges, potentials, and future directions," *IEEE Communications Magazine*, vol. 61, no. 1, pp. 40–46, 2023.

[5] S. Aditya, O. Dizdar, B. Clerckx, and X. Li, "Sensing using coded communications signals," *IEEE Open Journal of the Communications Society*, vol. 4, pp. 134–152, 2023.

[6] C. Aydogdu, M. F. Keskin, and H. Wymeersch, "Automotive radar interference mitigation via multi - hop cooperative radar communications," in *2020 17th European Radar Conference (EuRAD)*, pp. 270–273, 2021.

[7] H. Friis, "A note on a simple transmission formula," *Proceedings of the IRE*, vol. 34, no. 5, pp. 254–256, 1946.

[8] M. A. Richards, *Fundamentals of Radar Signal Processing*. McGraw-Hill Professional, 2005.

[9] Z. Yun and M. F. Iskander, "Ray tracing for radio propagation modeling: Principles and applications," *IEEE Access*, vol. 3, pp. 1089–1100, 2015.

[10] J. Taylor and A. Terzuoli, "On the concept of near field radar cross section," in *IEEE Antennas and Propagation Society International Symposium 1997. Digest*, vol. 2, pp. 1172–1175 vol.2, 1997.

[11] P. Pouliguen and L. Desclos, "A physical optics approach to near field RCS computations," in *Annales des télécommunications*, vol. 51, pp. 219–226, 1996.

[12] P. Pouliguen, J. F. Damiens, R. Hemon, and J. Saillard, "RCS computation in near field," in *DAYS on DIFFRACTION 2006*, pp. 252–265, 2006.

[13] S. Legault, "Refining physical optics for near-field computations," *Electronics Letters*, vol. 40, no. 1, p. 1, 2004.

[14] R. Deban, H. Boutayeb, J. Conan, and K. Wu, "Numerical and experimental analysis of metallic plate near-field RCS at oblique incidence and applications to radar systems," in *2009 Loughborough Antennas & Propagation Conference*, pp. 441–444, 2009.

[15] R. Deban, H. Boutayeb, K. Wu, and J. Conan, "Deterministic approach for spatial diversity analysis of radar systems using near-field radar cross section of a metallic plate," *IEEE Transactions on Antennas and Propagation*, vol. 58, no. 3, pp. 908–916, 2010.

[16] J. M. Tamayo-Palau and P. de Resseguier, "Simulation of near field RCS to reproduce measurement condition," in *2018 15th European Radar Conference (EuRAD)*, pp. 103–106, 2018.

[17] H.-T. Chou, W.-J. Gao, J. Zhou, B. You, and X.-H. He, "Enhancing electromagnetic backscattering responses for target detection in the near zone of near-field-focused phased array antennas," *IEEE Transactions on Antennas and Propagation*, vol. 69, no. 3, pp. 1658–1669, 2021.

[18] A. Elfrgani and C. J. Reddy, "Near-field RCS for automotive radar applications," in *2019 International Workshop on Antenna Technology (iWAT)*, pp. 217–220, 2019.

[19] A. Lahuerta-Lavieja, M. Johansson, U. Gustavsson, T. A. H. Bressner, and G. A. E. Vandenbosch, "Computationally efficient millimeter-wave backscattering models: A single-scattering model," *IEEE Transactions on Antennas and Propagation*, vol. 68, no. 8, pp. 6306–6316, 2020.

[20] A. Lahuerta-Lavieja, M. Johansson, C. Larsson, U. Gustavsson, and G. A. E. Vandenbosch, "Computationally efficient millimeter-wave scattering models: A multiple-scattering model," *IEEE Transactions on Antennas and Propagation*, vol. 70, no. 9, pp. 8250–8261, 2022.

[21] F. De Saint Moulin, K. A. Khalifeh, C. Craeye, L. Vandendorpe, and C. Oestges, "Novel electromagnetic-based radar propagation model for vehicular sensing," *IEEE Access*, vol. 12, pp. 128201–128214, 2024.

[22] F. Miller, A. Vandome, and J. McBrewster, *Fermat's Theorem (Stationary Points): Theorem, Real Analysis, Pierre de Fermat, Maxima and Minima, Derivative, Open Set, Stationary Point, Equation, Necessary and Sufficient Condition, Inflection Point, Second Derivative*. Alphascript Publishing, 2009.